CO_2 and glacial cycles

SIR — Although global ice volume variations of near-100,000-year period are clearly the dominant mode of glacial variability in the late Pleistocene[1], there is still no widely accepted explanation for this phenomenon. It is recognized, for example, that while Earth-orbital (Milankovitch) radiative cycles are the likely explanation of the near-20,000- and 40,000-year period ice variations, they are certainly not sufficient to explain the much larger 100,000-year variations (though arguments have been made that they may be necessary). In one model, Milankovitch forcing acts only to set the phase chronology of the 100,000-year variation, but its existence and large amplitude is a consequence of a free nonlinear oscillator driven by an internal instability of the carbon dioxide–ice volume–deep ocean circulation system[2,3]. A fundamental prediction of this model is that the 100,000-year ice volume cycle must be out of phase with atmospheric CO_2, higher CO_2 values being associated with decreasing ice volume, and vice versa.

To test this prediction we can invoke two widely accepted, independent measures of CO_2 and ice volume: the Vostok core-trapped air measurements[4,5]; and the SPECMAP $\delta^{18}O$ estimate[6], respectively. Although questions arise concerning the absolute chronologies of these two measures, it is of interest to examine their implications taking them at face value as the best estimates currently available. Some support for these estimates is provided by recent studies with regard to CO_2 (ref. 7) and to ice volume[8].

In the figure we show the phase-plane trajectory of these two variables. If CO_2 and ice volume were in-phase, the trajectories would overlap, forming a straight line and indicating a diagnostic relation between the two. But in fact the trajectories tend to form two main 100,000-year period loops with a clockwise flow, signifying a phase lag between the two variables such that high CO_2 is associated with decreasing ice volume and lower CO_2 with increasing ice volume, as predicted. Smaller loops are also present, particularly during the time of lower CO_2, which have shorter periods corresponding to the Milankovitch obliquity and precessional cycles. These smaller loops can be either clockwise or counterclockwise, indicating randomness in the sign of the phase lag between CO_2 and ice mass on these shorter timescales. Because little direct orbital forcing exists at the 100,000-year period, and the thermal effect of a 100 p.p.m. change in CO_2 concentration is as large as that due to the Milankovitch radiative changes at 65 °N that presumably drive the near-20,000- and 40,000-year cycles[9,10], it is implied that CO_2 can provide the internal forcing necessary to drive the main near 100,000-year cycles.

From another viewpoint, the 'hole' in the 100,000-year period loop represents a region of phase space from which the climate system tends to be driven, indicative of a region where an unstable equilibrium might be located. On the other hand, points along the main trajectory, particularly where their density is great, are indicative of more stable regions of the climate system.

It will be of great interest to extend the trajectory shown in the figure backwards in time as further Vostok CO_2 measurements projected to extend to 500,000 years before present[5] become available, and to repeat this mode of analysis for other measures of ice volume[8] or other revised estimates of the ice volume chronology that might turn out to be more accurate than SPECMAP.

Barry Saltzman
Mikhail Verbitsky
Department of Geology & Geophysics,
Yale University,
PO Box 6666,
New Haven,
Connecticut 06511, USA

1. Imbrie, J. *et al. Paleoceanography* (in the press).
2. Saltzman, B. *Clim. Dynam.* **1**, 77–85 (1987).
3. Saltzman, B. & Maasch, K. *Global Biogeochem. Cycles* **2**, 177–185 (1988).
4. Barnola, J. M. *et al. Nature* **329**, 408–414 (1987).
5. Jouzel, J. *et al. Nature* **364**, 407–412 (1993).
6. Imbrie, J. *et al.* in *Milankovitch and Climate* part I (eds Berger, A. *et al.*) 269–305 (Reidel, Dordrecht, 1984).
7. Shackleton, N. J. *et al. Quat. Sci. Rev.* **11**, 387–400 (1992).
8. Sowers, T. *et al. Paleoceanography* **6**, 679–696 (1991).
9. Oglesby, R. J. & Saltzman, B. *Geophys. res. Lett.* **17**, 1089–1092 (1990).
10. Saltzman, B. & Maasch, K. *Clim. Dynam.* **5**, 201–210 (1991).

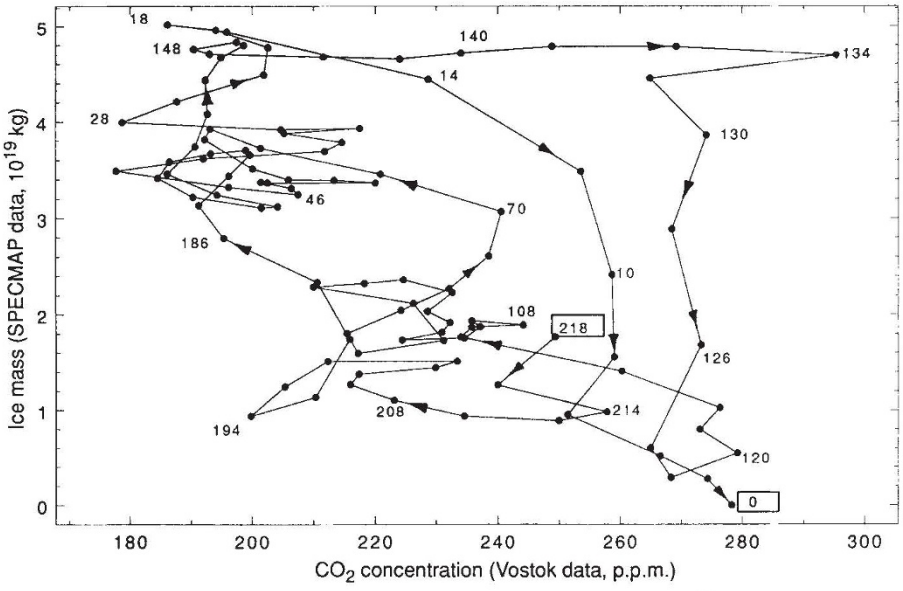

Evolution of the global climate system in the phase plane of ice mass (10^{19} kg) as deduced from the SPECMAP reconstruction[6] and carbon dioxide concentration as deduced from the Vostok ice core[5]. Numerals mark time (× 1,000 years before present), beginning at t=218,000 years before present and ending at the present, t=0 (boxed). Each dot represents a 2,000-year time step. Arrows point in the direction of decreasing age towards the present.

Urothelial carcinogenesis

SIR — Transitional cell carcinoma is a major genitourinary neoplasm arising from urothelial cells lining the bladder, ureter and renal pelvis. The frequent deletion of chromosome 9 in superficial carcinomas of this type has suggested that the condition begins by the functional inactivation of a putative tumour-suppressor gene. In attempting to localize this gene, we have applied the polymerase chain reaction (PCR)-based analysis of polymorphic simple sequence repeats or microsatellites to define regions of allelic loss on chromosome 9 in transitional cell carcinomas (ref. 1). Serendipitously, the use of these genetic markers has revealed another mechanism of urothelial carcinogenesis.

From a panel of 37 bladder, 3 ureter and 1 renal pelvis transitional cell carcinomas, we observed variations in the electrophoretic mobility of $(CA)_n \cdot (GT)_n$ microsatellite alleles in DNAs from a superficial ureter lesion (case 36), and an invasive ureter lesion (case 39), relative to DNAs from autologous peripheral blood lymphocytes. In case 36, we found mutant alleles at 16 (73%) of 22 loci on 4 of 5 chromosomes tested. The DNA from case 36, for example, was unaltered at D9S15, truncated at the argininosuccinate synthetase locus, and expanded at D10S89, D15S120 and D21S156 (*a* in the figure). In